TLR7 inhibition limits cardiac ischemic injury by disrupting ITGAM-dependent immune–endothelial interaction

Yijia Li[1], Yang Yang[1], Chanhee Park[1], Boyang Ren[1], Ruoxing Li[2], Amol Shetty[3], Brittney Williams[1], Ziyi Li[2], Lin Zou[1], Wei Chao[1#]

[1] Center for Shock, Trauma and Anesthesiology Research, University of Maryland School of Medicine, Baltimore, MD, 21201

[2] Department of Biostatistics, The University of Texas MD Anderson Cancer Center, Houston, TX, 77030

[3] Institute for Genome Sciences, University of Maryland School of Medicine, Baltimore, MD 21201

Corresponding author:

Wei Chao, MD, PhD
Email: wchao@som.umaryland.edu

Address:

Center for Shock, Trauma and Anesthesiology Research
University of Maryland School of Medicine
20 Penn Street, Suite S003, HSF-2
Baltimore, MD, 21201

ABSTRACT

Percutaneous coronary intervention (PCI) limits ischemic myocardial infarction but also triggers ischemia-reperfusion (I/R) injury in part driven by innate immune activation. Here, we identify Toll-like receptor 7 (TLR7), an endosomal sensor of single-stranded RNA, as a mediator of post-ischemic inflammation and myocardial damage. Pharmacological inhibition of TLR7 with enpatoran reduced myocardial inflammation and infarct size and improved cardiac function in a mouse model of I/R injury when administered before, during, or shortly after ischemia. Single-nucleus RNA sequencing revealed coordinated post-I/R expansion of myeloid cells and a distinct inflammatory endothelial subset enriched for leukocyte-interaction programs, with marked upregulation of *Itgam* in cardiac leukocytes and endothelial cells and in circulating monocytes. Circulating *ITGAM*$^{+}$ monocytes were similarly increased in patients with ST-segment elevation myocardial infarction 24 hours after coronary stenting. Mechanistically, TLR7 activation induced ITGAM expression in endothelial cells and leukocytes and promoted their adhesion via ITGAM-ICAM1 interaction under physiological shear stress, whereas ITGAM neutralization disrupted this interaction, reduced immune cell infiltration, and limited ischemic injury. These findings define a TLR7–ITGAM signaling axis as a key driver of endothelial–leukocyte crosstalk in myocardial I/R injury and support TLR7 inhibition as a promising therapeutic strategy to mitigate acute myocardial infarction.

One Sentence Summary: TLR7 inhibition attenuates cardiac ischemic injury by disrupting an ITGAM-dependent endothelial–leukocyte inflammatory axis.

Keywords: TLR7, enpatoran, single-nucleus RNA sequencing, Myocardial ischemia-reperfusion injury, ICAM1-ITGAM

INTRODUCTION

Cardiovascular disease, such as acute coronary syndrome, remains the leading cause of death and leads to immense health and economic burdens worldwide(*1*). In the U.S., about 805,000 people experience a heart attack every year. Of these, 605,000 are a first heart attack(*2*). The current reperfusion therapy, such as percutaneous coronary intervention (PCI) (*e.g.,* stenting), remains the most effective strategy to limit myocardial infarct (MI) size and preserve cardiac function(*3, 4*). However, reperfusion itself can paradoxically cause damage to myocardium, termed ischemia-reperfusion (I/R) injury(*4*), which is associated with subsequent lethal cardiovascular events, such as recurrent MI, arrhythmia, and cardiac arrest in 5-6% of patients who have undergone PCI(*3, 4*). Therefore, new cardiac protective strategies for lethal reperfusion injury are urgently needed.

Myocardial I/R injury is a complex process driven by multiple mechanisms(*4, 5*), including injurious innate immune activity in response to cell-released damage-associated molecular patterns (DAMPs)(*6-8*) such as extracellular (ex) nucleic acids. Studies have shown that myocardial I/R triggers the release of cellular nucleic acids into the cardiac interstitial space(*9*) and numerous miRNAs into blood circulation(*10*). Tissue RNA isolated from human and rodent hearts or plasma miRNAs identified via RNA array in mice with ischemic MI prove to be inflammatory and act via Toll-like receptor 7(TLR7)(*10-12*). Administration of RNase(*13, 14*) or a specific nucleic acid-binding nanoprobe(*9*) before and during ischemia reduces cell-free RNA and confers cardioprotection against I/R injury with reduced inflammation, smaller infarct size, and improved left ventricular function. Notably, a related paradigm is seen in autoimmune diseases, including systemic lupus erythematosus (SLE), rheumatoid arthritis, and psoriasis, in which self ex-RNA activates TLR7–mediated signaling(*15, 16*). Ex-RNA has been targeted for potential treatment of SLE in recent clinical trial(*17*). Patients with these autoimmune disorders exhibit a significantly higher risk of ischemic MI, likely attributed to chronic inflammation, endothelial dysfunction, and unstable atherosclerotic plaques(*18, 19*). Taken together, these observations support the hypothesis that ex-RNA-driven innate immune signaling mediates myocardial inflammation and contributes to reperfusion injury during I/R.

Expressed across immune and non-immune cells, mouse TLR7, or human TLR8, is a single-stranded RNA (ssRNA) sensor located in endosomes that recognizes certain extracellular miRNAs(*20-22*) and viral RNAs(*23, 24*). TLR7 activation elicits inflammatory cytokines, chemokines, and type I interferons. In the heart, local injection of miR-146a-5p directly triggers TLR7-dependent myocardial inflammation and cardiomyocyte dysfunction(*12*), and TLR7 is involved in adverse LV remodeling after MI in mice(*25*). TLR7 signaling is also reportedly associated with autoimmune myocarditis(*26*), conduction abnormalities(*27*). Yet the mechanistic role of TLR7 in cardiac I/R injury remains unknown.

In this study, we tested the therapeutic potential of the selective TLR7/8 antagonist enpatoran in a mouse model of I/R injury using dosing regimens that model clinically relevant reperfusion scenarios encountered in patients with acute myocardial infarction. To elucidate underlying mechanisms, we applied single-nucleus RNA sequencing (snRNA-seq) to define changes in myocardial cellular composition and cell type–specific transcriptional programs following I/R and TLR7 inhibition. This approach uncovered coordinated expansion of myeloid cells and a distinct inflammatory endothelial subset enriched for leukocyte-interaction pathways, with prominent upregulation of *Itgam* in cardiac leukocytes and endothelial cells. Complementary in vitro and in vivo studies demonstrated that TLR7 activation promotes leukocyte–endothelial adhesion through induction of the ITGAM–ICAM1 axis under physiological shear stress, whereas ITGAM neutralization attenuated immune cell infiltration and reduced ischemic myocardial injury. Together, these findings establish TLR7 as a druggable upstream regulator of immune–endothelial crosstalk

in myocardial I/R injury and support TLR7 inhibition as a translational strategy to limit cardiac ischemic injury.

RESULTS

Plasma small RNA-seq identifies an increase in proinflammatory miRNAs after myocardial I/R injury

In a mouse model of cardiac I/R injury(*9, 13*), there was a substantial increase in plasma RNA at 24 hours (**Fig. 1A**). RNA-seq revealed that miRNAs were the predominant small RNA species in plasma, accounting for 82% of total RNA reads in control animals (**Fig. 1B**). Among the 1,915 annotated mouse miRNAs in miRBase, 508 miRNAs were detected with ≥10 raw reads. Of these, 7 miRNAs–miR-29c-5p, miR-3061-3p, miR-741-3p, miR-8116, miR-1843-5p, miR-5113, and miR-8097–were significantly upregulated by >1.5-fold ($P < 0.05$) in the I/R mice as compared with sham controls (**Fig. 1C**). Notably, four of these miRNAs (miR-29c-5p, miR-3061-3p, miR-741-3p, and miR-8116) harbored at least one of the five UU-rich motifs predictive for pro-inflammatory activity(*21*) (**Fig. 1C, Table S1**), three of them elicited a dose-dependent MIP-2 production in bone marrow-derived macrophages (BMDMs), an effect that was completely blocked by the TLR7 antagonist enpatoran (**Fig. 1D**).

Enpatoran, a selective TLR7/8 antagonist, protects the heart from I/R injury

Given the contribution of ex-RNA and multiple proinflammatory miRNAs to innate inflammation and myocardial I/R injury, we reasoned that targeting the downstream RNA sensor TLR7 would be more efficacious than individual plasma miRNAs. To test this, we examined the effect of enpatoran, a selected TLR7/8 antagonist recently developed by Merck KGaA for treatment of autoimmune diseases(*28*), in a mouse model of cardiac I/R injury. Each mouse received two intraperitoneal injections of enpatoran (5 mg/kg) or saline, two hours apart. Four dosing regimens centered around 45 min of ischemia were adopted (**Fig. 2A**):(1) *Prevention (PP)*: 1st dose given 1 hour before ischemia (45 min); (2) *Treatment (TP)*: 1st dose at 35 minutes during ischemia; (3) *Early rescue (ERP)*: 1st dose at 30 minutes after ischemia; and (4) *Late rescue (LRP)*: 1st dose at 2 hours after ischemia. Enpatoran markedly reduced MI size in the groups of PP, TP, and ERP protocols, achieving 35–76% reductions in myocardial infarction/area-at-risk (MI/AAR), whereas the LRP protocol provided no protection (**Fig. 2B-E**). Area-at-risk was similar across groups (**Fig. 2C**), demonstrating that ischemic areas were unchanged in the different treatment groups. Plasma cTnI levels were reduced by ~70% with enpatoran (**Fig. 2F**), further validating the robust cardioprotection by TLR7 inhibition. Baseline echocardiographic parameters were comparable across groups (**Table S2**). I/R injury caused ventricular dilation and impaired systolic and diastolic function, accompanied by reduced cardiac output (CO), LV ejection fraction (LVEF), global longitudinal strain (GLS), and radial strain (GRS), and increased left atrial (LA) size and mitral valve E wave velocity and reversed longitudinal strain rate ratio (E/e′ sr) (**Fig. 2G-O**). Enpatoran administered in the PP, TP, or ERP regimens significantly improved cardiac structure and function, restoring CO, LVEF, GLS, and GRS and reducing LA dilation and E/e′ sr (**Fig. 2G-O**). In contrast, the LRP regimen failed to improve cardiac performance, consistent with the absence of infarct-sparing effect. Of note, enpatoran had no adverse effects on cardiac function in sham mice, and echocardiographic parameters were comparable between the treatment groups (**Table S3**).

To determine whether enpatoran-induced cardioprotection is mediated by TLR7 inhibition, age-matched WT and TLR7-deficient (TLR7 KO) mice underwent I/R injury and received enpatoran or saline following the TP protocol (**Fig. S1A**). Like enpatoran-treated WT mice, TLR7 KO mice had significantly reduced MI/LV and MI/AAR ratios compared with WT mice treated with saline.

However, enpatoran provided no additional MI-sparing effect in TLR7 KO mice (**Fig. S1B–C**), indicating that its cardioprotective effects are TLR7-dependent. Baseline echocardiographic parameters were comparable across groups (**Table S4**). After I/R, NS-treated WT mice developed severe systolic and diastolic dysfunction, including reduced CO, LVEF, and GLS, and increased LA diameter and E/e′ sr (**Fig. S1D–H**). In contrast, NS-TLR7 KO and Enpa-TLR7 KO mice showed similarly preserved cardiac function, further confirming that enpatoran acts through TLR7 inhibition. Of note, comparable cardioprotection was observed in female mice treated with enpatoran (**Fig. S2, Table S5**). Specifically, both enpatoran treatment and TLR7 deficiency significantly reduced infarct size and preserved systolic and diastolic cardiac function after I/R in female mice, as assessed by echocardiographic parameters. Collectively, these results demonstrate that TLR7 inhibition by enpatoran confers a robust, time-sensitive cardioprotection against ischemic MI in a TLR7-dependent manner.

snRNA-seq reveals expansion of myeloid and endothelial cells with distinct transcriptomic signatures after I/R injury

Given the central role of innate immune activation in cardiac I/R injury, we first analyzed the temporal dynamics of cardiac immune cell infiltration and cytokine expression between 24 hours to 14 days after I/R injury. Flow cytometry revealed a rapid innate immune response, with $Ly6G^{+}$ neutrophils peaking at 24 hours and $Ly6C^{high}$ monocytes peaking between 24 and 72 hours, whereas $Ly6C^{low}$ monocytes and $F4/80^{+}$ macrophages remained relatively stable over time (**Fig. S3A–B**). Consistently, IL-6– and TNFα–expressing neutrophils and $Ly6C^{high}$ monocytes peaked at 24 and 72 hours, respectively, while cytokine-positive $Ly6C^{low}$ monocytes exhibited a delayed increase (**Fig. S3C–D**).

Next, we performed snRNA-seq of LV tissues collected at 24 hours after surgery from NS-Sham, NS-I/R, and enpatoran-I/R mice. High-quality nucleus preparations yielded 18,133, 20,432, and 18,201 nuclei of combined three samples in each group, respectively (**Table S6**). As shown in **Fig. 3A**, cardiac cells were visualized using Uniform Manifold Approximation and Projection (UMAP) by group information. I/R injury resulted in a significant reduction in cardiomyocytes compared with sham-operated controls. The total number of endothelial cells (ECs) was largely unchanged; however, an EC subcluster with transcriptional features proximal to infiltrating neutrophils and monocytes on the UMAP (EC8) was significantly expanded. In parallel, cardiac immune cells, including neutrophils and monocytes, were markedly increased after I/R. Notably, enpatoran treatment substantially preserved cardiomyocyte abundance and reduced neutrophil and monocyte infiltration compared with NS-treated I/R mice (**Fig. 3A, Table S7**). Furthermore, KEGG pathway analysis identified multiple innate immune and proinflammatory pathways across endothelial and myeloid compartments after I/R, including leukocyte transendothelial migration, regulation of actin cytoskeleton, hematopoietic cell lineage, cytokine receptor interaction, chemokine signaling, some of which were attenuated in response to enpatoran treatment (**Table S8**). These data demonstrate that TLR7 signaling drives the coordinated expansion of myeloid cells and an endothelial subset with distinct transcriptional reprogramming following myocardial I/R.

Itgam expression is upregulated in cardiac cells and in circulating monocytes after I/R

Among genes associated with these proinflammatory pathways, *Itgam* exhibited an impressive upregulation following I/R injury and downregulation to enpatoran treatment in EC8 (I/R vs. Sham: 16-fold; Enpa-I/R vs. NS-I/R: 2.7-fold), monocytes (I/R vs. Sham: 4.0-fold; Enpa-I/R vs. NS-I/R: 1.7-fold), and neutrophils (Enpa-I/R vs. NS-I/R: 1.7-fold). ITGAM is a critical subunit of the Mac-1

integrin complex (CD11b/CD18) predominantly expressed in neutrophils and monocytes but also in endothelial cells(*29-31*) and involved in various immune functions, including leukocyte adhesion, migration, phagocytosis, and several immunological disorders(*32*), mainly through the binding of the I-domain of ITGAM to ligands like ICAM-1(*33*). The abundance of Itgam$^+$ cells was significantly increased in the EC8, neutrophil, and monocyte clusters (**Fig. 3B**). Density-Expression plot further revealed an increased proportion of Itgam$^+$ cells within these cell clusters, accompanied by elevated overall *Itgam* expression in the I/R group (**Fig. 3C**). These transcriptional changes were corroborated at the protein level by immunofluorescence analysis, which revealed increased *Itgam* expression in myocardial CD31$^+$ endothelial cells, Ly6G$^+$ neutrophils, and CCR2$^+$ monocytes following I/R injury (**Fig. 3D and Fig. S4–S6**). In sham-operated hearts, endothelial cells exhibited an intact, well-organized vascular architecture with minimal immune cell infiltration or *Itgam* expression. In contrast, I/R injury disrupted endothelial organization and myocardial structure, with markedly increased ITGAM$^+$ endothelial cells and enhanced infiltration of ITGAM$^+$ neutrophils and monocytes. Enpatoran treatment reversed these effects, significantly reducing ITGAM expression in cardiac endothelial cells, neutrophils, and monocytes (**Fig. 3B–D**). To determine whether cardiac I/R induces systemic leukocyte expansion and ITGAM expression, we analyzed leukocytes from peripheral blood, spleen, and bone marrow. Circulating neutrophil numbers increased rapidly within 2 hours after I/R, while monocyte numbers modestly decreased at 4 hours. (**Fig. S7A-B**). Importantly, ITGAM expression in circulating monocytes was significantly increased between 2-4 hours after I/R, which was reversed by enpatoran treatment (**Fig. S7B**). No significant alterations were observed in the spleen or bone marrow, with the exception of a modest increase in splenic neutrophils and a concomitant decrease in splenic monocytes after I/R (**Fig. S8**).

To assess *ITGAM* expression in human leukocytes, we re-analyzed a previously published single-cell RNA-seq dataset from patients with acute MI(*34*). The proportion of monocytes within peripheral blood mononuclear cells (PBMCs) was significantly increased in patients with STEMI and further expanded 24 hours after stent placement compared with healthy controls. As anticipated, TLR8 was highly expressed compared to *TLR7* in human monocytes; both receptors share functional similarities in endosomal RNA sensing and innate immune activation. Importantly, like mouse blood monocytes, monocytes from STEMI patients were increased in % *ITGAM+* numbers as well as level of *ITGAM* expression, which was further increased after coronary stenting (**Fig. 3E**). Together, these results indicate that myocardial I/R induces TLR7-dependent ITGAM upregulation across cardiac endothelial cells, neutrophils, and monocytes, as well as in circulating monocytes

TLR7 activation promotes *Itgam* expression and endothelial–immune cell crosstalk

To determine whether TLR7 activation is sufficient to induce *Itgam* expression, bone marrow–derived macrophages (BMDMs) and human coronary artery endothelial cells (HCAECs) were treated with the TLR7/8 agonists R837, R848, or miR-146a-5p, an inflammatory miRNA that binds to and activates TLR7(*20*) (**Fig. 4A**). R837 increased *Itgam* expression in BMDMs at 6 and 18 hours, accompanied by an increase in IL-6 production (**Fig. 4B–C**). Confocal immunofluorescent microscopy demonstrated marked increases in ITGAM protein expression in both BMDMs and HCAECs following TLR7/8 stimulation (**Fig. 4D–4G**). To assess the functional consequences of TLR7/8 activation, we used a microfluidic adhesion assay to quantify human EC (HCAECs)–monocyte (THP-1) adhesion under physiological shear stress. R848 treatment of either HCAECs or THP-1 monocytes increased endothelial–monocyte adhesion to a similar extent, whereas concurrent stimulation of both cell types resulted in a significantly greater increase in monocyte adhesion (**Fig. S9**) (**videos S1–S2**). Notably, R848-induced endothelial–monocyte adhesion was markedly attenuated by enpatoran treatment, confirming a TLR7/8-mediated process (**Fig. 5A–**

B). To determine the contribution of ITGAM to R848-induced endothelial–monocyte crosstalk, an ITGAM-neutralizing antibody was applied to either HCAECs or THP-1 monocytes after R848 stimulation. Blocking ITGAM on THP-1 monocytes reduced adhesion to endothelial cells by 85.8% (**videos S3**), whereas ITGAM blockade on HCAECs produced a more modest reduction of 51.9% (**Fig. 5C–D, videos S4**). Concurrent ITGAM blockade in both cell types resulted in the greatest reduction in endothelial–monocyte adhesion (**videos S5**), suggesting that both EC and monocyte ITGAM plays a significant role, but monocyte-expressed ITGAM plays a more dominant role, in mediating TLR7-induced monocyte–endothelial interactions. Similar results were observed in human neutrophil–EC interaction (**Fig. 5E–F)**. Together, these results suggest that TLR7 activation enhances endothelial–Mo/NE functional crosstalk through an ITGAM-dependent mechanism.

ITGAM neutralization attenuates cardiac leukocyte infiltration and confers protection against myocardial I/R injury

To determine whether ITGAM contributes to post-ischemia inflammation and injury after I/R, mice were treated with an ITGAM-neutralizing antibody (ITGAM Ab) or an isotype control antibody (100 µg per mouse, i.p.) 1 hour before ischemia (**Fig. 6A**). Mice receiving ITGAM antibody exhibited significantly smaller infarct as evidenced by reduced MI/LV and MI/AAR ratios (**Fig. 6B–C**) and improved systolic (better LVEF, CO, and GLS) and diastolic (smaller LA dilation and a lower E/e′ sr ratio) functions as compared with the controls (**Fig. 6D–H, and Table S9).** ITGAM Ab treatment also markedly reduced infiltration of neutrophils and monocytes after I/R injury (**Fig. 6I–L**). These results support the notion that ITGAM expression, driven by I/R and mediated by TLR7 signaling, plays an important role in post-ischemia myocardial inflammation and injury.

Enhanced ICAM1-ITGAM interaction after I/R injury

Leukocyte adhesion to the endothelium is a critical driver of myocardial inflammation following I/R injury(*35*). To delineate the molecular mechanisms underlying this endothelial–leukocyte crosstalk in vivo, we performed *in silico* ligand–receptor (L–R) interaction analyses using our cardiac snRNA-seq dataset and quantified expressed L–R pairs among major cardiac cell types. Among 2,377 identified L–R pairs, 24 were significantly upregulated after I/R and reversed by enpatoran treatment specifically in endothelial cell–monocyte (EC–Mo) or endothelial cell–neutrophil (EC–NE) interactions (**Fig. 7A**). Most of these L-R pairs are functionally linked with inflammatory processes, including leukocyte adhesion (ICAM1–ITGAM), chemotactic recruitment (CXCL2–CXCR2), and immune–vascular signaling (SEMA7A–[ITGB1+ITGA1]). Notably, the ICAM1–ITGAM emerged as a prominent pair, as it was upregulated after I/R and attenuated by enpatoran treatment in both EC–Mo and EC–NE interactions. Given the central role of leukocyte–endothelial adhesion in post-ischemic inflammation, we further examined regulation of the ICAM1–ITGAM axis across relevant cardiac cell populations. Unlike *Itgam*, which was upregulated in endothelial cells, neutrophils, and monocytes after I/R and attenuated by enpatoran treatment (**Fig. 3B–D, Fig. S10A**), Icam1 expression was increased in endothelial cells, predominantly in EC4 and EC5, compared with neutrophils and monocytes after I/R and was not significantly affected by enpatoran (**Fig. S10B–C**).

To determine whether these transcriptional changes translated into physical molecular interactions, we performed STED super-resolution immunofluorescence imaging on myocardial sections. Following I/R injury, ITGAM^{+} leukocytes were frequently observed in close apposition to ICAM1^{+} endothelial cells, with discrete ICAM1–ITGAM interaction sites at cell-to-cell interfaces (**Fig. 7B, middle panel, Video S6**). In addition, colocalization and close proximity of ICAM1 and

ITGAM was detected within endothelial junctional membrane protrusions, structures that have been reported to serve as hotspots for neutrophil transmigration(*36*) (**Fig. 7B, lower panel, Videos S7**). In contrast, sham hearts contained a small number of ITGAM-expressing leukocytes without detectable ITGAM–ICAM1 leukocyte–endothelial contacts (**Fig. 7B, Fig. S11, Video S8**). Together, these findings suggest that myocardial I/R enhances ICAM1–ITGAM interaction and endothelial–leukocyte crosstalk, a process regulated by TLR7 signaling.

TLR7 regulates ICAM1 expression and leukocyte-endothelium adhesion

To determine whether TLR7/8 activation is sufficient to induce ICAM1 expression, BMDMs and HCAECs were treated with the TLR7/8 agonists R837 or R848, or with miR-146a-5p. Confocal immunofluorescence microscopy revealed a significant increase in ICAM1 expression as quantified as total integrated fluorescence intensity in BMDMs and HCAECs treated with R837, R848, or miR-146a-5p compared with untreated controls (**Fig. 8A–B**). To assess the functional contribution of ICAM1 to leukocyte–endothelial interactions, an ICAM1-neutralizing antibody was applied to either THP-1 monocytes or HCAECs following R848 stimulation. ICAM1 blockade on HCAECs markedly reduced THP-1 adhesion (**Videos S9**), whereas ICAM1 blockade on THP-1 cells resulted in a very modest reduction (**Fig. 8C–D, Videos S10**). Simultaneous ICAM1 blockade in both cell types produced the greatest inhibition of monocyte adhesion, indicating that endothelial ICAM1 plays a dominant role in mediating TLR7-induced monocyte–endothelial interactions (**Videos S11**). A similar inhibitory pattern was observed in human neutrophil adhesion assays (**Fig. 8E–F**). Collectively, these findings demonstrate that TLR7 signaling is sufficient to induce ICAM1 expression and acts upstream of coordinated ITGAM and ICAM1 induction, thereby promoting enhanced leukocyte–endothelial crosstalk.

DISCUSSION

In this study, we uncover a previously unrecognized role for Toll-like receptor 7 (TLR7) as a central innate immune sensor that links ischemia–reperfusion (I/R) injury to pathological leukocyte–endothelial interactions in the heart. Using single-nucleus transcriptomics, we identify coordinated expansion of cardiac myeloid cells and a distinct endothelial cell (EC) population enriched for inflammatory and leukocyte adhesion programs following I/R. Among these shared responses, *Itgam*, encoding the leukocyte adhesion receptor CD11b, emerged as a convergent and conserved signature, increased not only in cardiac immune and endothelial compartments after I/R but also in circulating monocytes from mice and from patients with STEMI 24 hours after coronary stenting. Functionally, pharmacologic inhibition of TLR7 with the selective TLR7/8 antagonist enpatoran reduced infarct size and improved cardiac function across a clinically relevant therapeutic window encompassing pre-, peri-, and early post-ischemic administration. Mechanistically, TLR7 activation drove leukocyte–endothelial adhesion by promoting coordinated induction of ITGAM and ICAM1, whereas TLR7 inhibition or ITGAM neutralization disrupted this interaction, attenuated myocardial inflammation, and limited post-ischemia MI. Together, these findings position TLR7 as a druggable upstream regulator of leukocyte–endothelial adhesion and suggest that targeting innate immune RNA sensing may represent an effective strategy to limit cardiac ischemic injury during reperfusion therapy.

Previous studies have shown that myocardial I/R promotes the release of cellular RNA and miRNAs into the extracellular space and that removal of extracellular RNA (ex-RNA) confers cardioprotection, implicating ex-RNA as a mediator of myocardial injury (*9, 11, 13, 14*). Consistent with these observations, plasma bulk RNA-seq in the present study revealed increased circulating miRNAs, several of which exerted potent proinflammatory effects through TLR7-dependent

signaling. In parallel, snRNA-seq of myocardium analyses identified *Tlr7* as one of the most highly expressed Toll-like receptors in the post-I/R heart (Fig. S12). Both pharmacologic inhibition and genetic deletion of TLR7 markedly attenuated post-ischemia myocardial injury. Enpatoran, a selective TLR7/8 antagonist developed by Merck KGaA(*28*), has demonstrated a favorable safety profile in humans(*37*) and efficacy in phase 2 clinical trials for autoimmune disease(*38*). To model clinically relevant reperfusion scenarios after a heart attack, we evaluated multiple dosing regimens spanning pre-ischemic, peri-ischemic, and early post-ischemic administration. Enpatoran significantly reduced infarct size and preserved left ventricular function when administered before ischemia, during ischemia, or shortly after reperfusion; this benefit was absent in TLR7-deficient mice, confirming TLR7-dependent efficacy, not an off-target benefit. In contrast, protection was lost when treatment was delayed until 2 hours after reperfusion, underscoring a narrow therapeutic window for TLR7-mediated I/R injury. These findings are consistent with prior reports linking TLR7 to adverse long-term post–MI remodeling and other cardiac diseases such as myocarditis(*26*), conduction abnormalities(*27*), and adverse post–myocardial infarction remodeling(*25*).

To determine an appropriate time window for mechanistic interrogation, we performed a pilot time-course analysis of cardiac inflammatory cell dynamics from 1 to 14 days after I/R or sham surgery. The data confirmed that neutrophils and proinflammatory monocytes peaked between 24 and 72 hours after I/R. snRNA-seq at 24 hours demonstrated a marked shift in cardiac cellular composition, characterized by a reduction in cardiomyocytes and robust expansion of immune cell populations, particularly neutrophils and monocytes, consistent with prior reports (*39-42*). In contrast, the overall endothelial cell (EC) population was largely preserved. A key observation, however, was the selective expansion of a distinct endothelial subpopulation, EC8, which increased from ~0.3% of total cardiac cells at baseline to ~3.6% after I/R. EC8 localized in close proximity to neutrophils and monocytes on UMAP projections demonstrating a pronounced proinflammatory and immune-interactive program that closely mirrored infiltrating innate immune cells, suggesting coordinated endothelial–immune reprogramming during post-ischemic inflammation. Importantly, both immune cell infiltration and EC8 expansion were markedly attenuated by enpatoran treatment, thus linking TLR7 to these downstream events. Together, these findings identify a TLR7-dependent inflammatory endothelial state that emerges during I/R and provide a cellular framework connecting innate immune RNA sensing to immune–endothelial crosstalk in myocardial I/R injury.

Moreover, transcripts associated with leukocyte transendothelial migration pathway were selectively upregulated in EC8 after I/R and attenuated by enpatoran treatment. Among these genes, *Itgam* emerged as a particularly compelling candidate, as its expression was robustly induced by I/R and consistently suppressed by TLR7 inhibition across myocardial EC8, neutrophils, and monocytes. *Itgam* encodes the αM subunit of the Mac-1 integrin complex, a key regulator of immune cell adhesion, migration, and phagocytosis (*43-47*), largely through binding of its I-domain to ligands such as ICAM1(*33*). The shared, TLR7-dependent induction of *Itgam* across endothelial and myeloid compartments therefore supports ITGAM as a convergent molecular effector linking innate immune sensing to immune–endothelial interactions during I/R. Beyond the myocardium, myocardial I/R was associated with an increased proportion of Itgam-expressing circulating monocytes in mice and in patients with STEMI, both prior to and 24 hours after coronary stenting, suggesting that the TLR7-dependent upregulation of Itgam identified in cardiac cells is also reflected in peripheral blood monocytes. Although the exact functional significance of this finding in circulating monocytes remains unclear, one possibility is that elevated cellular Itgam expression facilitates the recruitment of circulating monocytes to the heart during reperfusion.

A key finding of the current study is that TLR7 emerged as a critical upstream regulator of leukocyte–endothelial adhesion through coordinated control of the ICAM1–ITGAM communication. *In silico* L-R pair analyses based on snRNA-seq of the heart uncovered dynamic change in *Icam1–Itgam* communication between EC, mainly EC4 and EC5 subpopulations, and leukocyte after I/R and in response to enpatoran treatment, which was supported by super-resolution STED imaging at cell-cell interface and within endothelial junctional membrane protrusions in I/R heart. *In vitro*, TLR7 activation was sufficient to induce robust ITGAM and ICAM1 expression in immune and endothelial cells and to enhance leukocyte–endothelial adhesion under physiological shear stress, whereas neutralizing antibody studies identified leukocyte-expressed ITGAM and EC-associated ICAM1 as the dominant determinant of leukocyte-endothelial interaction. These findings were further supported in vivo, where ITGAM neutralization significantly reduced neutrophil and monocyte infiltration and limited post-ischemia MI size, although the relative contributions of neutrophil-, monocyte-, and endothelial–specific ITGAM are unclear and will require future investigation.

Several limitations of this study warrant consideration. *In vivo* experiments were conducted in young, healthy mice, which do not fully reflect the clinical complexity of myocardial infarction, where aging and cardiometabolic comorbidities may influence innate immune signaling and therapeutic responsiveness. Since both pharmacologic TLR7 inhibition and antibody-mediated ITGAM neutralization modulate the global TLR7-ITGAM pathway, the relative contributions of endothelial-, neutrophil-, and monocyte-derived TLR7–ITGAM axis to leukocyte–endothelial adhesion and I/R injury remain unresolved and will require further investigation using cell–type–specific genetic approaches.

In conclusion, our findings identify TLR7 as a central innate immune RNA sensor that mechanistically links I/R–induced immune activation to endothelial dysfunction and myocardial injury. By coordinating ICAM1–ITGAM expression and engagement, TLR7 signaling drives leukocyte recruitment and sustains post-ischemic inflammatory responses. Pharmacologic inhibition of TLR7 disrupted immune–endothelial interactions, limited infarct expansion, and preserved cardiac function within a defined therapeutic window. Together, these data position the TLR7–ITGAM axis as a pivotal regulator of endothelial–leukocyte crosstalk in myocardial I/R injury and highlight TLR7 signaling as a promising target for therapeutic intervention in acute MI.

MATERIALS AND METHODS

Study Design

We hypothesized that Toll-like receptor 7 (TLR7), a sensor of single-stranded RNA, mediates myocardial I/R injury. To test this, we first performed bulk plasma RNA sequencing to identify miRNAs upregulated after myocardial I/R and assessed their ability to induce MIP-2 production in a TLR7-dependent manner. We then evaluated the therapeutic efficacy of pharmacologic TLR7 inhibition in a well-established murine model of cardiac I/R injury. The selective TLR7/8 antagonist enpatoran was administered before, during, or after ischemia to model clinically relevant timing relative to coronary reperfusion therapy. Myocardial infarct size and cardiac function were assessed by histochemical staining and echocardiography to define the temporal window during which TLR7 blockade attenuates reperfusion injury.

To elucidate downstream mechanisms regulated by TLR7 signaling during reperfusion, we performed snRNA-seq on cardiac tissue from WT mice subjected to sham surgery or I/R with or without enpatoran treatment. This unbiased approach enabled systematic identification of cell compositions and cell–type–specific transcriptional programs associated with reperfusion injury. To establish translational relevance, we analyzed publicly available single-cell transcriptomic

datasets of blood monocytes from patients with STEMI following coronary stenting, focusing on the expression of *Itgam*, *Tlr7*, and *Tlr8*.

We next performed mechanistic and functional validation studies to define how TLR7 activation regulates leukocyte–endothelial crosstalk. Using *in vitro* systems, including BMDMs. THP-1 monocytes, and HCAECs, we tested whether selective TLR7 activation was sufficient to induce adhesion molecule expression. Expression of ITGAM and ICAM1 was quantified using ImageXpress automated cell imaging. Functional consequences of TLR7 activation were assessed using a microfluidic adhesion assay under physiological shear stress, in which monocytes or neutrophils were perfused over endothelial monolayers with or without pharmacologic TLR7 inhibition. To delineate cell–type–specific contributions, neutralizing antibodies targeting ITGAM or ICAM1 were applied selectively to leukocytes or ECs to evaluate their relative roles in mediating adhesion.

Guided by snRNA-seq findings, we further performed *in silico* ligand–receptor interaction analyses using CellChat to identify adhesion-related interactions among immune and endothelial cell populations, with particular focus on the ICAM1–ITGAM pair. These predicted interactions were subsequently validated at the molecular level using super-resolution stimulated emission depletion (STED) microscopy to directly visualize ICAM1–ITGAM interactions at leukocyte–endothelial interfaces and within cells on sliced myocardium.

For all *in vivo* studies, mice were randomly assigned to treatment groups, and investigators performing surgeries, administering treatments, and analyzing data were blinded to genotype and treatment allocation. Sample sizes were determined by power analysis to achieve 80% power (two-sided $P < 0.05$) with a minimum detectable effect size comparable to prior I/R studies. All animal experiments were conducted in accordance with protocols approved by the Institutional Animal Care and Use Committee of the University of Maryland School of Medicine.

Statistical analysis

Statistical analyses were performed using GraphPad Prism (v10.4.0; GraphPad Software, La Jolla, CA), R (v4.3.0), and relevant bioinformatics packages as specified below. Continuous variables are presented as mean ± SEM unless otherwise indicated. Normality was assessed where appropriate. For comparisons between two groups, Student's t test or the Mann–Whitney U test was used as appropriate. For comparisons involving more than two groups, one-way ANOVA followed by Tukey's post hoc test was applied. For experiments involving multiple treatment protocols and interventions, two-way ANOVA was used to assess the effects of treatment and protocol, followed by appropriate post hoc testing.

RNA sequencing data analysis

snRNA-seq data underwent quality control and computation of gene-barcode matrices using the Cell Ranger pipeline (10x Genomics) with default parameters. Gene-barcode matrices were imported into Seurat (v4.3.0) and underwent integration, batch effect correction, and normalization for downstream analysis. Low-quality nuclei were filtered based on read depth, gene complexity, and mitochondrial content to remove potential doublets or damaged nuclei. Raw UMI counts were normalized using Seurat's SCTransform workflow, and highly variable genes were identified for downstream analyses. Dimensionality reduction was performed using principal component analysis (PCA), followed by Uniform Manifold Approximation and Projection (UMAP) was used for clustering of individual cells. Cell clustering identification was conducted using the Louvian community detection algorithm in Seurat, and cluster-specific marker genes were identified using the marker analysis (FindAllMarkers function, default parameters). Cell type annotation was based on comparison of cluster-specific marker genes to cell type–specific genes from literature and public databases. Differential gene expression was assessed between IR and

treatment conditions using the Wilcoxon method implemented in Seurat. Functional enrichment analyses of differentially expressed genes were performed against KEGG pathway annotations to identify enrichment of signaling programs and cellular processes.

Plasma small RNA sequencing data were processed and normalized using DESeq (21.48.2) to identify differentially expressed miRNAs across experimental groups. Cell–cell communication analyses were inferred using ligand–receptor interaction models implemented in the CellChat-v2 R package, which enables quantification of intercellular signaling strength and visualization of inferred communication networks across cellular compartments. Unless stated otherwise, a two-sided P value < 0.05 was considered statistically significant for all computational analyses.

List of Supplementary Materials

1. Supplemental Materials and Methods

2. Supplemental Tables:

Table S1. Upregulated plasma miRNA after cardiac I/R injury

Table S2. Detailed echocardiography data (baseline vs. post-I/R) in four treatment protocols

Table S3. Detailed baseline echocardiography data in control sham mice with the Prevention Protocol

Table S4. Detailed echocardiography data (baseline and post-I/R) in WT and TLR7 KO male mice

Table S5. Detailed echocardiography data (baseline and post-I/R) in female WT and KO mice

Table S6. Quality assessment of nucleus preparations for snRNA-seq

Table S7. Nucleus number and percentage (cluster nuclei / total nuclei x 100%) of each cell cluster

Table S8. KEGG pathway analysis – enriched transcriptomic signatures of EC8, monocytes, and neutrophils

Table S9. Detailed echocardiography data (baseline and post-I/R) in male mice treated with ITGAM and control antibody

Table S10. Global marker genes

3. Supplemental Figures

Figure S1. Enpatoran-induced cardioprotection in ischemic MI is TLR7-dependent

Figure S2. TLR7 KO and Enpatoran treatment reduce MI sizes and preserve cardiac function after I/R in female mice.

Figure S3. Temporal dynamics of cardiac immune cell infiltration and cytokine-expressing cells after I/R injury.

Figure S4. ITGAM expression in endothelial cells.

Figure S5. ITGAM expression in neutrophils.

Figure S6. ITGAM expression in monocytes.

Figure S7. Blood neutrophil and monocyte dynamics and ITGAM expression following myocardial I/R injury.

Figure S8. Spleen and bone marrow neutrophil and monocyte dynamics and ITGAM expression following I/R injury.

Figure S9. Microfluidic adhesion assay of THP-1 adhesion to HCAEC.

Figure S10. *Itgam* and *Icam1* expression level/.

Figure S11. STED super-resolution imaging of endothelial cells in the normal heart.

Figure S12. snRNA-seq reveals TLR family gene expressions across various cardiac cell types.

Figure S13. Detailed snRNA-seq analysis data.

4. Legends for Videos 1 to 11

Video S1–S5 (.mp4 format). Microfluidic adhesion assay of THP-1 adhesion to HCAEC under different treatment conditions: **1:** non-treatment control; **2:** R848 treatment for both Mo and EC; **3:** R848 for both Mo and EC, with ITGAM-neutralizing antibody applied only to Mo; **4:** R848 for both Mo and EC, with ITGAM-neutralizing antibody applied only to EC; **5:** R848 and ITGAM-neutralizing antibody applied to both Mo and EC. EC, endothelial cell; Mo, monocyte.

Video S6–S8 (.mp4 format). STED super-resolution 3D imaging: immunofluorescence staining of heart sections showing ITGAM (red), ICAM1 (green), and cell membranes (WGA, magenta) in I/R cell–cell interface (**6**), I/R endothelial cells (**7**), and Sham heart (**8**).

Video S9–S11 (.mp4 format). Microfluidic adhesion assay of THP-1 adhesion to HCAEC under different treatment conditions: **9:** R848 for both Mo and EC, with ICAM1-neutralizing antibody applied only to Mo; **10:** R848 for both Mo and EC, with ICAM1-neutralizing antibody applied only to EC; **11:** R848 and ICAM1-neutralizing antibody applied to both Mo and EC. EC, endothelial cell; Mo, monocyte.

REFERENCES

1. S. S. Martin, A. W. Aday, Z. I. Almarzooq, C. A. M. Anderson, P. Arora, C. L. Avery, C. M. Baker-Smith, B. B. Gibbs, A. Z. Beaton, A. K. Boehme, Y. Commodore-Mensah, M. E. Currie, M. S. V. Elkind, K. R. Evenson, G. Generoso, D. G. Heard, S. Hiremath, M. C. Johansen, R. Kalani, D. S. Kazi, D. Ko, J. Liu, J. W. Magnani, E. D. Michos, M. E. Mussolino, S. D. Navaneethan, N. I. Parikh, S. M. Perman, R. Poudel, M. Rezk-Hanna, G. A. Roth, N. S. Shah, M.-P. St-Onge, E. L. Thacker, C. W. Tsao, S. M. Urbut, H. G. C. V. Spall, J. H. Voeks, N.-Y. Wang, N. D. Wong, S. S. Wong, K. Yaffe, L. P. Palaniappan, 2024 Heart Disease and Stroke Statistics: A Report of US and Global Data From the American Heart Association. *Circulation* **149**, e347–e913 (2024).
2. CDC, Heart Disease Facts. https://www.cdc.gov/heart-disease/data-research/facts-stats/index.html#:~:text=Heart%20attack,3. **2024**, (2024).
3. A. Bagai, G. D. Dangas, G. W. Stone, C. B. Granger, Reperfusion strategies in acute coronary syndromes. *Circulation research* **114**, 1918–1928 (2014).
4. D. M. Yellon, D. J. Hausenloy, Myocardial reperfusion injury. *N Engl J Med* **357**, 1121–1135 (2007).
5. S. Verma, P. W. M. Fedak, R. D. Weisel, J. Butany, V. Rao, A. Maitland, R.-K. Li, B. Dhillon, T. M. Yau, Fundamentals of Reperfusion Injury for the Clinical Cardiologist. *Circulation* **105**, 2332–2336 (2002).
6. R. I. Jaen, A. Val-Blasco, P. Prieto, M. Gil-Fernandez, T. Smani, J. L. Lopez-Sendon, C. Delgado, L. Bosca, M. Fernandez-Velasco, Innate Immune Receptors, Key Actors in Cardiovascular Diseases. *JACC Basic Transl Sci* **5**, 735–749 (2020).
7. A. Anzai, S. Ko, K. Fukuda, Immune and Inflammatory Networks in Myocardial Infarction: Current Research and Its Potential Implications for the Clinic. *Int J Mol Sci* **23**, (2022).
8. W. Chao, Toll-like receptor signaling: a critical modulator of cell survival and ischemic injury in the heart. *Am J Physiol Heart Circ Physiol* **296**, H1–12 (2009).
9. H. H. Chen, H. Yuan, H. Cho, Y. Feng, S. Ngoy, A. T. Kumar, R. Liao, W. Chao, L. Josephson, D. E. Sosnovik, Theranostic Nucleic Acid Binding Nanoprobe Exerts Anti-inflammatory and Cytoprotective Effects in Ischemic Injury. *Theranostics* **7**, 814–825 (2017).
10. Y. Feng, L. Zou, D. Yan, H. Chen, G. Xu, W. Jian, P. Cui, W. Chao, Extracellular MicroRNAs Induce Potent Innate Immune Responses via TLR7/MyD88-Dependent Mechanisms. *J Immunol* **199**, 2106–2117 (2017).
11. Y. Feng, H. Chen, J. Cai, L. Zou, D. Yan, G. Xu, D. Li, W. Chao, Cardiac RNA induces inflammatory responses in cardiomyocytes and immune cells via Toll-like receptor 7 signaling. *J Biol Chem* **290**, 26688–26698 (2015).
12. B. K. Shimada, Y. Yang, J. Zhu, S. Wang, A. Suen, S. M. Kronstadt, A. Jeyaram, S. M. Jay, L. Zou, W. Chao, Extracellular miR-146a-5p Induces Cardiac Innate Immune Response and Cardiomyocyte Dysfunction. *Immunohorizons* **4**, 561–572 (2020).
13. C. Chen, Y. Feng, L. Zou, L. Wang, H. H. Chen, J. Y. Cai, J. M. Xu, D. E. Sosnovik, W. Chao, Role of extracellular RNA and TLR3-Trif signaling in myocardial ischemia-reperfusion injury. *J Am Heart Assoc* **3**, e000683 (2014).
14. H. A. Cabrera-Fuentes, M. Ruiz-Meana, S. Simsekyilmaz, S. Kostin, J. Inserte, M. Saffarzadeh, S. P. Galuska, V. Vijayan, I. Barba, G. Barreto, S. Fischer, G. Lochnit, O. N.

Ilinskaya, E. Baumgart-Vogt, A. Böning, S. Lecour, D. J. Hausenloy, E. A. Liehn, D. Garcia-Dorado, K. D. Schlüter, K. T. Preissner, RNase1 prevents the damaging interplay between extracellular RNA and tumour necrosis factor-α in cardiac ischaemia/reperfusion injury. *Thromb Haemost* **112**, 1110–1119 (2014).

15. Z. Yang, S. Ji, L. Liu, S. Liu, B. Wang, Y. Ma, X. Cao, Promotion of TLR7-MyD88-dependent inflammation and autoimmunity in mice through stem-loop changes in Lnc-Atg16l1. *Nat Commun* **15**, 10224 (2024).

16. S. L. Schell, K. N. Bricker, A. J. Fike, S. B. Chodisetti, P. P. Domeier, N. M. Choi, M. J. Fasnacht, S. A. Luckenbill, S. F. Ziegler, Z. S. M. Rahman, Context-Dependent miR-21 Regulation of TLR7-Mediated Autoimmune and Foreign Antigen-Driven Antibody-Forming Cell and Germinal Center Responses. *J Immunol* **206**, 2803–2818 (2021).

17. D. J. Burge, V. P. Werth, S. A. Boackle, J. Posada, Evaluation of RNase therapy in systemic lupus erythematosus: a randomised phase 2a clinical trial of RSLV-132. *Lupus Sci Med* **11**, (2024).

18. M. S. Garshick, N. L. Ward, J. G. Krueger, J. S. Berger, Cardiovascular Risk in Patients With Psoriasis: JACC Review Topic of the Week. *J Am Coll Cardiol* **77**, 1670–1680 (2021).

19. A. Rahman, Systemic lupus erythematosus: managing cardiovascular risk factors. *Lancet Rheumatol* **6**, e415–e416 (2024).

20. S. Wang, Y. Yang, A. Suen, J. Zhu, B. Williams, J. Hu, F. Chen, R. Kozar, S. Shen, Z. Li, A. Jeyaram, S. M. Jay, L. Zou, W. Chao, Role of extracellular microRNA-146a-5p in host innate immunity and bacterial sepsis. *iScience* **24**, 103441 (2021).

21. B. Ren, R. Li, C. Y. Lin, C. Park, S. Wang, A. O. Suen, J. Kessler, S. Yang, R. Kozar, L. Zou, B. Williams, Z. Li, P. Hu, W. Chao, Nucleotide motif-guided selection of plasma microRNA biomarkers in trauma. *iScience* **28**, 113569 (2025).

22. B. Williams, R. Kozar, W. Chao, EMERGING ROLE OF EXTRACELLULAR RNA IN INNATE IMMUNITY, SEPSIS, AND TRAUMA. *Shock* **59**, 190–199 (2023).

23. J. M. Lund, L. Alexopoulou, A. Sato, M. Karow, N. C. Adams, N. W. Gale, A. Iwasaki, R. A. Flavell, Recognition of single-stranded RNA viruses by Toll-like receptor 7. *Proc Natl Acad Sci U S A* **101**, 5598–5603 (2004).

24. F. Heil, H. Hemmi, H. Hochrein, F. Ampenberger, C. Kirschning, S. Akira, G. Lipford, H. Wagner, S. Bauer, Species-specific recognition of single-stranded RNA via toll-like receptor 7 and 8. *Science* **303**, 1526–1529 (2004).

25. D. P. V. de Kleijn, S. Y. Chong, X. Wang, S. Yatim, A. M. Fairhurst, F. Vernooij, O. Zharkova, M. Y. Chan, R. S. Y. Foo, L. Timmers, C. S. P. Lam, J. W. Wang, Toll-like receptor 7 deficiency promotes survival and reduces adverse left ventricular remodelling after myocardial infarction. *Cardiovasc Res* **115**, 1791–1803 (2019).

26. M. G. Hasham, N. Baxan, D. J. Stuckey, J. Branca, B. Perkins, O. Dent, T. Duffy, T. S. Hameed, S. E. Stella, M. Bellahcene, M. D. Schneider, S. E. Harding, N. Rosenthal, S. Sattler, Systemic autoimmunity induced by the TLR7/8 agonist Resiquimod causes myocarditis and dilated cardiomyopathy in a new mouse model of autoimmune heart disease. *Dis Model Mech* **10**, 259–270 (2017).

27. D. Alvarez, P. Briassouli, R. M. Clancy, J. Zavadil, J. H. Reed, R. G. Abellar, M. Halushka, K. Fox-Talbot, F. J. Barrat, J. P. Buyon, A Novel Role of Endothelin-1 in Linking Toll-like Receptor 7-mediated Inflammation to Fibrosis in Congenital Heart Block*. *Journal of Biological Chemistry* **286**, 30444–30454 (2011).

28. J. Vlach, A. T. Bender, M. Przetak, A. Pereira, A. Deshpande, T. L. Johnson, S. Reissig, E. Tzvetkov, D. Musil, N. T. Morse, P. Haselmayer, S. C. Zimmerli, S. L. Okitsu, R. L. Walsky, B. Sherer, Discovery of M5049: A Novel Selective Toll-Like Receptor 7/8 Inhibitor for Treatment of Autoimmunity. *J Pharmacol Exp Ther* **376**, 397–409 (2021).

29. M. A. Arnaout, Structure and function of the leukocyte adhesion molecules CD11/CD18. *Blood* **75**, 1037–1050 (1990).

30. K. Ley, C. Laudanna, M. I. Cybulsky, S. Nourshargh, Getting to the site of inflammation: the leukocyte adhesion cascade updated. *Nat Rev Immunol* **7**, 678–689 (2007).

31. L. Chen, Z. Shangguan, Z. Dong, Q. Deng, Y. Ding, S. Yang, NFIL3 aggravates human coronary artery endothelial cell injury by promoting ITGAM transcription in Kawasaki disease. *Hematology* **28**, 2277502 (2023).

32. S. C. Fagerholm, M. MacPherson, M. J. James, C. Sevier-Guy, C. S. Lau, The CD11b-integrin (ITGAM) and systemic lupus erythematosus. *Lupus* **22**, 657–663 (2013).

33. L. M. Uotila, M. Aatonen, C. G. Gahmberg, Integrin CD11c/CD18 α-chain phosphorylation is functionally important. *J Biol Chem* **288**, 33494–33499 (2013).

34. I. V. van Blokland, R. Oelen, H. E. Groot, J. W. Benjamins, K. Pekayvaz, C. Losert, V. Knottenberg, M. Heinig, L. Nicolai, K. Stark, P. van der Harst, L. Franke, M. G. P. van der Wijst, Single-Cell Dissection of the Immune Response After Acute Myocardial Infarction. *Circulation: Genomic and Precision Medicine* **17**, e004374 (2024).

35. A. K. Kakkar, D. J. Lefer, Leukocyte and endothelial adhesion molecule studies in knockout mice. *Current Opinion in Pharmacology* **4**, 154–158 (2004).

36. J. J. Arts, E. K. Mahlandt, M. L. Grönloh, L. Schimmel, I. Noordstra, E. Gordon, A. C. van Steen, S. Tol, B. Walzog, J. van Rijssel, M. A. Nolte, M. Postma, S. Khuon, J. M. Heddleston, E. Wait, T. L. Chew, M. Winter, E. Montanez, J. Goedhart, J. D. van Buul, Endothelial junctional membrane protrusions serve as hotspots for neutrophil transmigration. *Elife* **10**, (2021).

37. A. Port, J. V. Shaw, L. Klopp-Schulze, A. Bytyqi, C. Vetter, E. Hussey, N. Mammasse, V. Ona, A. Bachmann, D. Strugala, C. Reh, K. Goteti, Phase 1 study in healthy participants of the safety, pharmacokinetics, and pharmacodynamics of enpatoran (M5049), a dual antagonist of toll-like receptors 7 and 8. *Pharmacol Res Perspect* **9**, e00842 (2021).

38. L. Klopp-Schulze, S. Gopalakrishnan, O. Yalkinoglu, Y. Kuroki, H. Lu, K. Goteti, A. Krebs-Brown, M. Nogueira Filho, U. Gradhand, M. Fluck, J. Shaw, J. Dong, K. Venkatakrishnan, Asia-Inclusive Global Development of Enpatoran: Results of an Ethno-Bridging Study, Intrinsic/Extrinsic Factor Assessments and Disease Trajectory Modeling to Inform Design of a Phase II Multiregional Clinical Trial. *Clin Pharmacol Ther* **115**, 1346–1357 (2024).

39. W. Lin, X. Chen, D. Wang, R. Lu, C. Zhang, Z. Niu, J. Chen, X. Ruan, X. Wang, Single-nucleus ribonucleic acid-sequencing and spatial transcriptomics reveal the cardioprotection of Shexiang Baoxin Pill (SBP) in mice with myocardial ischemia-reperfusion injury. *Front Pharmacol* **14**, 1173649 (2023).

40. B. Molenaar, L. T. Timmer, M. Droog, I. Perini, D. Versteeg, L. Kooijman, J. Monshouwer-Kloots, H. de Ruiter, M. M. Gladka, E. van Rooij, Single-cell transcriptomics following ischemic injury identifies a role for B2M in cardiac repair. *Commun Biol* **4**, 146 (2021).

41. C. Zhong, H. Dong, Y. Ma, B. Zhuang, H. Shi, L. Hong, Single-cell sequencing combined with transcriptomics and in vivo and in vitro analysis reveals the landscape of ferroptosis in myocardial ischemia–reperfusion injury. *The FASEB Journal* **38**, e70164 (2024).

42. M. Cui, Z. Wang, K. Chen, A. M. Shah, W. Tan, L. Duan, E. Sanchez-Ortiz, H. Li, L. Xu, N. Liu, R. Bassel-Duby, E. N. Olson, Dynamic Transcriptional Responses to Injury of Regenerative and Non-regenerative Cardiomyocytes Revealed by Single-Nucleus RNA Sequencing. *Dev Cell* **53**, 102–116.e108 (2020).

43. M. Zhou, X. Wang, Y. Shi, Y. Ding, X. Li, T. Xie, Z. Shi, W. Fu, Deficiency of ITGAM Attenuates Experimental Abdominal Aortic Aneurysm in Mice. *Journal of the American Heart Association* **10**, e019900 (2021).

44. D. A. Solovjov, E. Pluskota, E. F. Plow, Distinct roles for the alpha and beta subunits in the functions of integrin alphaMbeta2. *J Biol Chem* **280**, 1336–1345 (2005).

45. M. A. Arnaout, R. F. Todd, 3rd, N. Dana, J. Melamed, S. F. Schlossman, H. R. Colten, Inhibition of phagocytosis of complement C3- or immunoglobulin G-coated particles and of C3bi binding by monoclonal antibodies to a monocyte-granulocyte membrane glycoprotein (Mol). *J Clin Invest* **72**, 171–179 (1983).

46. J. T. Avery, R. V. Jimenez, J. L. Blake, T. T. Wright, B. León-Ruiz, T. R. Schoeb, A. J. Szalai, D. C. Bullard, Mice expressing the variant rs1143679 allele of ITGAM (CD11b) show impaired DC-mediated T cell proliferation. *Mammalian Genome* **30**, 245–259 (2019).

47. S. Q. Khan, I. Khan, V. Gupta, CD11b Activity Modulates Pathogenesis of Lupus Nephritis. *Front Med (Lausanne)* **5**, 52 (2018).

ACKNOWLEDGMENTS

We thank Dr. S. Ament and Ms. M. Cortes of the Institute for Genome Sciences, University of Maryland School of Medicine, for expert assistance with nuclei isolation.

Funding: This work was funded by the National Institutes of Health (R35-GM140822 to W.C.), and Y.L. is supported by an American Heart Association Postdoctoral Fellowship (26POST1559348).

Author contributions: Conceptualization: W.C., L.Z., Y.L. Methodology: Y.L., Y.Y, C.P., B.R., R.L., A.S., and Z.L. Investigation: Y.L., Y.Y, C.P., B.R., R.L., A.S., and Z.L. Funding acquisition: W.C. Project administration: W.C., L.Z., B.W. Supervision: W.C., L.Z., B.W. Writing – draft: Y.L., W.C. Writing – review & editing: Y.L. C.P., B.R., R.L., B.W., Z.L., L.Z., and W.C.

Competing interests: A patent application related to the use of enpatoran for the treatment of cardiac ischemia–reperfusion injury has been filed (PCT/US2025/037133, “Methods of Treating Ischemia/Reperfusion Injury”). The authors declare that they have no competing interests.

Data and materials availability: Source data are provided and are deposited in the NIH GEO repository upon publication (plasma small RNA-seq: GSE148864; cardiac snRNA-seq: XXX). Additional datasets are available from the corresponding author upon request.

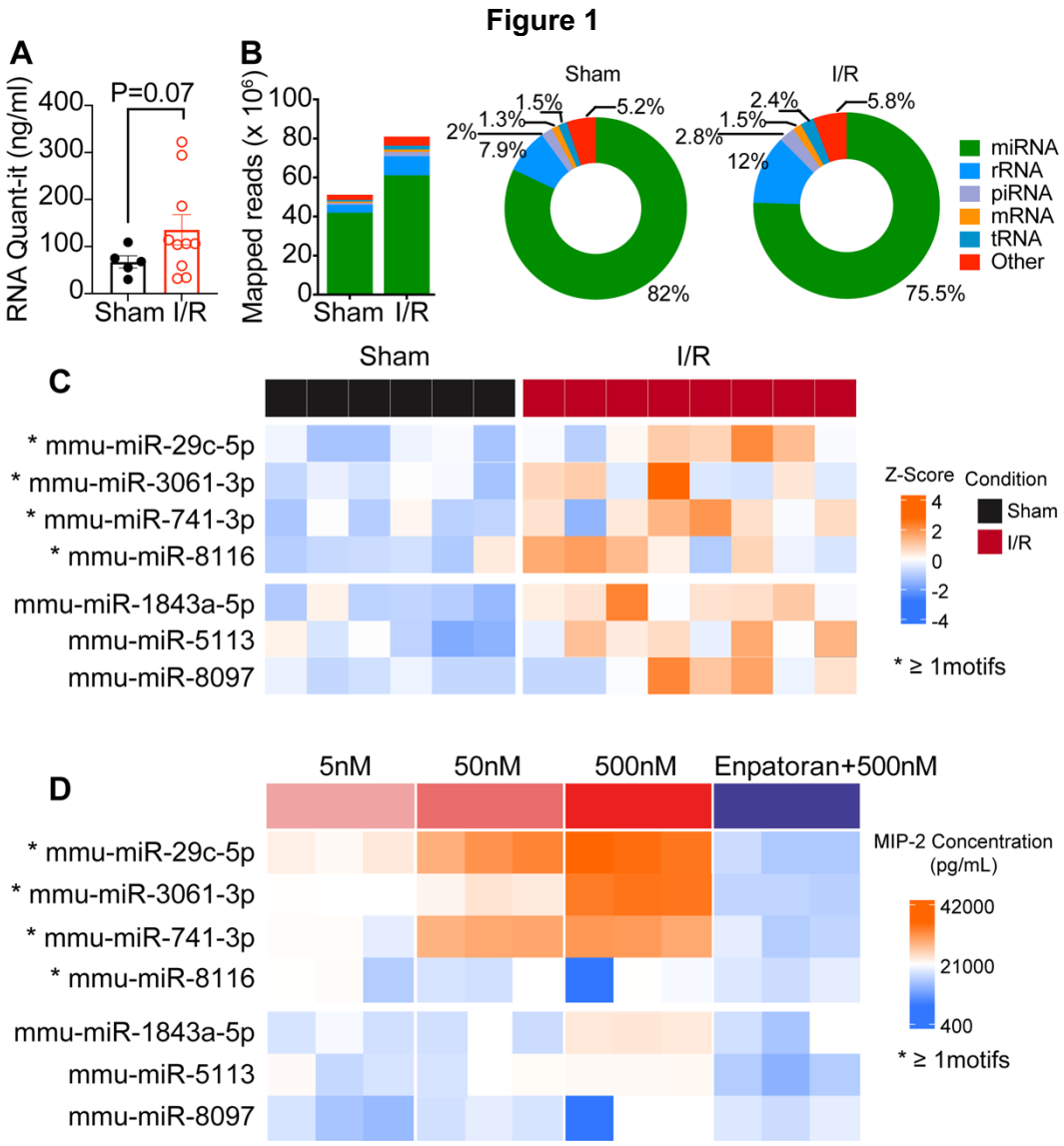

Figure 1. Plasma small RNA-seq and identification of proinflammatory miRNAs in a mouse model of MI. A, Plasma RNA quantifications 24 hours after Sham or I/R procedure (n=5-10). **B,** RNA-seq analysis with mapped read counts and relative percentage of different RNA biotypes in the plasma (n=6-8). **C,** Upregulated plasma miRNAs between I/R vs. Sham identified by RNA-seq. Four miRNAs contain at least one of the five proinflammatory motifs (.uuc; u..uu.; .a.....uu.; g.uu.; uu...u.). **D,** MIP-2 production in bone marrow-derived macrophages (BMDM) treated with miRNA mimics. I/R, ischemia-reperfusion**.** * Indicates miRNAs containing proinflammatory motifs in their sequences (see Table S1).

Figure 2

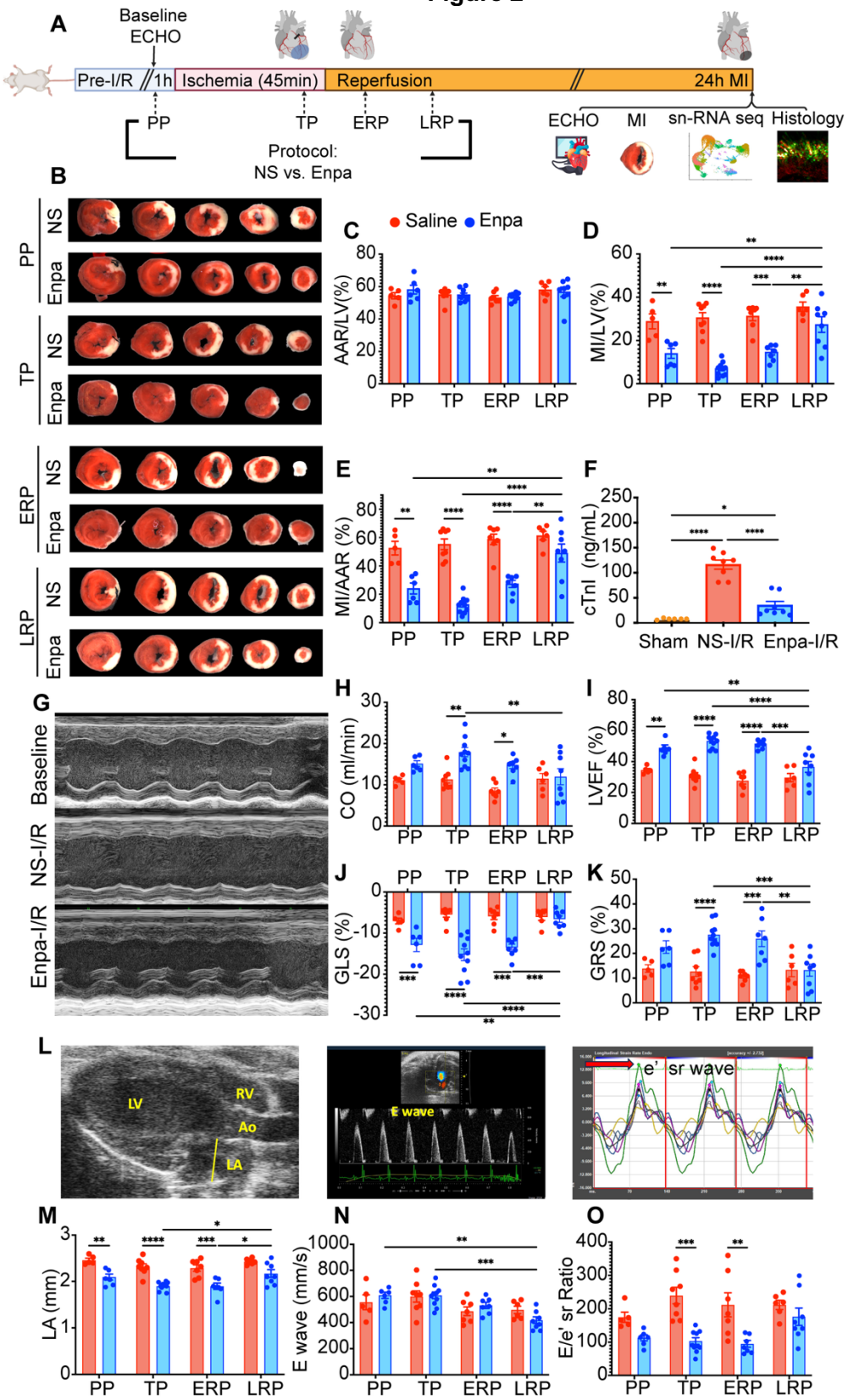
A
Baseline ECHO
Pre-I/R
1h
Ischemia (45min)
Reperfusion
24h MI
PP
TP
ERP
LRP
Protocol: NS vs. Enpa
ECHO
MI
sn-RNA seq
Histology
B
PP
TP
ERP
LRP
NS
Enpa
C
Saline
Enpa
AAR/LV(%)
D
MI/LV(%)
E
MI/AAR (%)
F
cTnI (ng/mL)
Sham
NS-I/R
Enpa-I/R
G
Baseline
NS-I/R
Enpa-I/R
H
CO (ml/min)
I
LVEF (%)
J
GLS (%)
K
GRS (%)
L
LV
RV
Ao
LA
E wave
e'
sr wave
M
LA (mm)
N
E wave (mm/s)
O
E/e' sr Ratio

Figure 2. Enpatoran reduces infarct size and preserves cardiac function after I/R. A, Study diagram for intraperitoneal administration of enpatoran in cardiac I/R model and experimental endpoints (n = 6-10 mice per group). For each protocol (PP, TP, ERP, or LRP), two doses of enpatoran (5 mg/kg) were administered 2 hours apart; the diagram shows the 1st dose. **B**, Representative TTC-stained images of MI. **C-E**, AAR/LV, MI/LV, and MI/AAR 24h after I/R. **F**, Plasma cTnI following I/R (PP protocol). **G**, M-mode images of echocardiography. **H-K**, Cardiac output (CO) (**H**), left ventricular ejection fraction (LVEF) (**I**), GLS (**J**), and GRS (**K**). **L**, B-mode images showing LA diameter (left panel), E waves (middle panel), and e' sr waves (right panel). **M-O**, Quantification of LA diameter (**M**), E wave velocity (**N**), and E/e' sr (**O**). Data shown are means ± SEM. One-way and two-way ANOVA were used to test statistical significance. *P < 0.05, **P < 0.01, ***P < 0.001, ****P < 0.0001. Enpa, enpatoran; NS, normal saline; I/R, ischemia-reperfusion; PP, prevention protocol; TP, treatment protocol; ERP, early rescue protocol; LRP, late rescue protocol; ECHO, echocardiography; AAR, area-at-risk; MI, myocardial infarction; RV, right ventricle; LA, left atrium; Ao, aorta; E wave, mitral valve E wave velocity; E/e' sr, mitral valve E wave velocity and reversed longitudinal strain rate ratio; GLS, global longitudinal strain; GRS, global radial strain; cTnI, Cardiac troponin I.

Figure 3

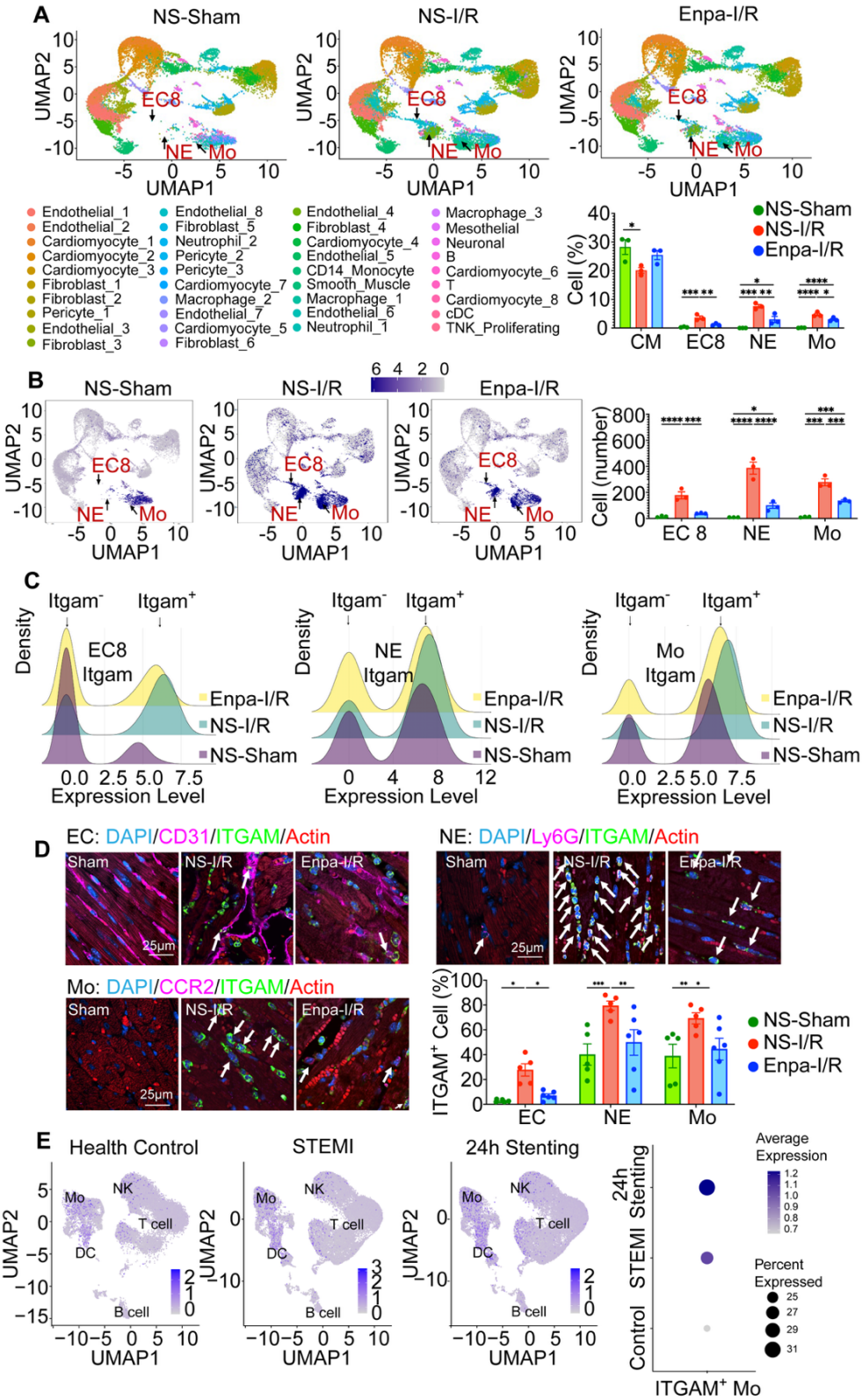
A
NS-Sham
NS-I/R
Enpa-I/R
UMAP2
UMAP1
EC8
NE
Mo
Endothelial_1
Endothelial_2
Cardiomyocyte_1
Cardiomyocyte_2
Cardiomyocyte_3
Fibroblast_1
Fibroblast_2
Pericyte_1
Endothelial_3
Fibroblast_3
Endothelial_8
Fibroblast_5
Neutrophil_2
Pericyte_2
Pericyte_3
Cardiomyocyte_7
Macrophage_2
Endothelial_7
Cardiomyocyte_5
Fibroblast_6
Endothelial_4
Fibroblast_4
Cardiomyocyte_4
Endothelial_5
CD14_Monocyte
Smooth_Muscle
Macrophage_1
Endothelial_6
Neutrophil_1
Macrophage_3
Mesothelial
Neuronal
B
Cardiomyocyte_6
T
Cardiomyocyte_8
cDC
TNK_Proliferating
Cell (%)
CM
EC8
NE
Mo
NS-Sham
NS-I/R
Enpa-I/R
B
Cell (number)
EC 8
C
Itgam⁻
Itgam⁺
Density
EC8 Itgam
NE Itgam
Mo Itgam
Expression Level
D
EC: DAPI/CD31/ITGAM/Actin
NE: DAPI/Ly6G/ITGAM/Actin
Mo: DAPI/CCR2/ITGAM/Actin
Sham
25μm
ITGAM⁺ Cell (%)
E
Health Control
STEMI
24h Stenting
NK
T cell
DC
B cell
Average Expression
Percent Expressed
ITGAM⁺ Mo

Figure 3. snRNA-seq reveals expansion of myeloid and endothelial cells with distinct transcriptomic signatures in ischemic MI. A, UMAP visualizing cardiac cell clusters (upper) and the percentage of CM, EC8, NE, and Mo among total cells (lower right) from three groups of male mice (n=3 per group). **B,** UMAP of Itgam$^+$ cells with *Itgam* expression levels shown by a light grey-to-dark purple gradient (log2-normalized expression; *left*). Quantification of Itgam$^+$ EC8, NE, and Mo was shown on the *right*. **C**, Density-Expression plot of *Itgam* in EC8 (*left*), NE (*middle*), and Mo (*right*). **D**, Representative immunofluorescent images of sarcomeric actin (*red*), CD31/Ly6G/CCR2 (*magenta*), and Itgam (*green*) of heart sections. Nuclei were stained with blue DAPI. The bar graph illustrates quantification of Itgam$^+$ EC, NE, and Mo (n=5-6 mice per group). **E,** UMAP of human blood mononuclear cells showing *ITGAM* expression. scRNA-seq analysis of monocyte *ITGAM* expression from healthy controls and STEMI patients before and after coronary reperfusion. Dot plots represent the percentage of ITGAM$^+$ monocytes among total mononuclear cells analyzed (n=38 patients per group). Data shown are means ± SEM. A one-way ANOVA was used to test for statistical significance. *P < 0.05, **P < 0.01, ***P < 0.001, ****P < 0.0001. NS, normal saline; Enpa, enpatoran; I/R, ischemia-reperfusion; CM, cardiomyocyte; EC, endothelial cell; NE, neutrophil; Mo, monocyte; UMAP, uniform manifold approximation and projection; DAPI, 4', 6-diamidino-2-phenylindole; STEMI, ST-segment elevation myocardial infarction; IF, Immunofluorescence.

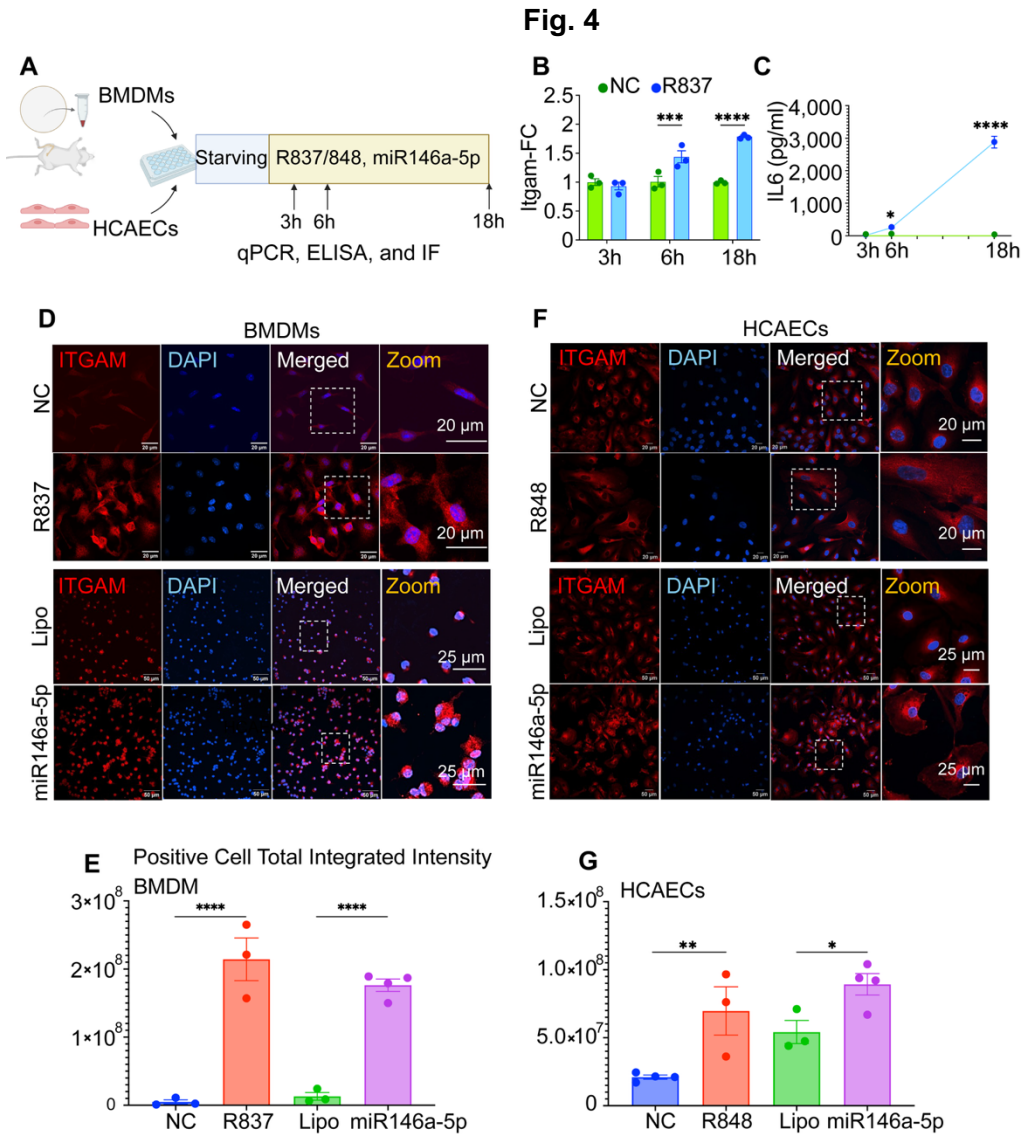

Figure 4. TLR7 activation increases *Itgam* expression in macrophages and endothelial cells. A, Experimental diagram of cell treatment with TLR7 agonists. **B,** Expression level of *Itgam* in BMDMs was examined by qRT-PCR. Relative expression of *Itgam* in the R837-treatment group was calculated with the non-treated control (NC). **C**, IL-6 production by BMDMs as measured by ELISA. **D & F**, The representative images of ITGAM expression in BMDMs (**D**) and HCAECs (**F**). **E & G,** Quantification of the ITGAM$^+$ cell total integrated intensity. Data shown are means ± SEM. A one-way ANOVA was used to test for statistical significance. *P < 0.05, **P < 0.01, ***P < 0.001, ****P < 0.0001. NC, nontreatment control; DAPI, 4′,6-diamidino-2-phenylindole; BMDMs, bone-marrow-derived macrophage; HCAEC, human coronary artery endothelial cell; FC, fold-change; lipo, lipofectamine; integrated intensity, the sum of pixel intensities within a designated area of a cell.

Fig. 5

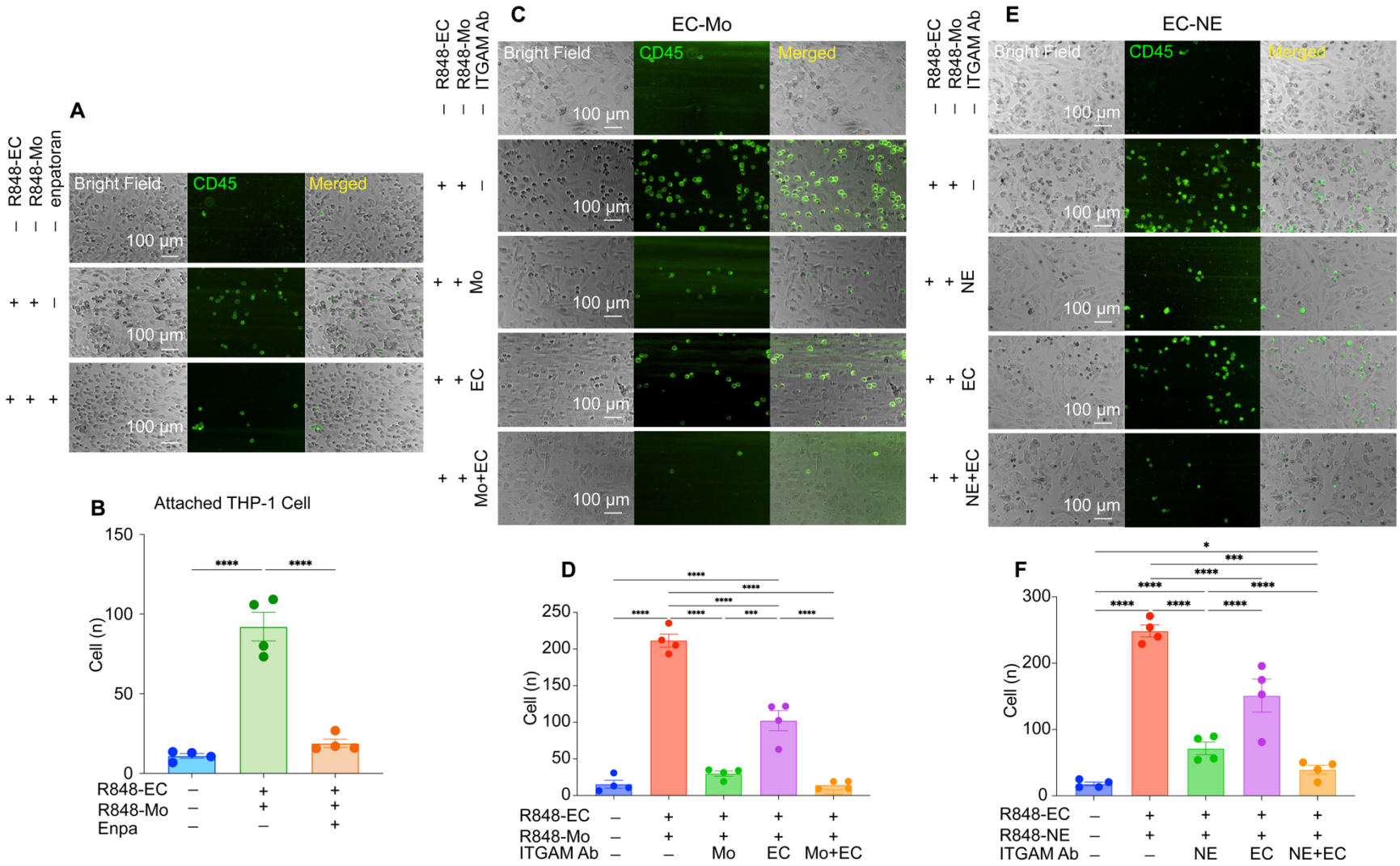
A
R848-EC
R848-Mo
enpatoran
Bright Field
CD45
Merged
100 μm
B
Attached THP-1 Cell
Cell (n)
R848-EC
R848-Mo
Enpa
C
EC-Mo
R848-EC
R848-Mo
ITGAM Ab
Mo
EC
Mo+EC
D
Cell (n)
R848-EC
R848-Mo
ITGAM Ab
Mo
EC
Mo+EC
E
EC-NE
NE
NE+EC
F
Cell (n)
R848-EC
R848-NE
ITGAM Ab
NE
EC
NE+EC

Figure 5. TLR7 activation increases leukocyte-endothelial adhesion. A, C, E, Microfluidic adhesion assay of THP-1 (Mo) or human fresh neutrophil adhesion to HCAEC under different treatment conditions as indicated (R848/enpatoran: 3h for Mo, 18h for EC; ITGAM Ab: 1h). **B, D, & F**, Quantification of THP-1 or human fresh neutrophil adhesion under different treatment conditions. $CD45^+$ immune cells are shown in green. Adherent $CD45^+$ cells appear as discrete green puncta, while continuous green streaks reflect perfused monocytes under flow conditions. Data shown are means ± SEM. A one-way ANOVA was used to test for statistical significance. *$P < 0.05$, ***$P < 0.001$, ****$P < 0.0001$. HCAEC, Human coronary artery endothelial cell; NE, neutrophil; Mo, monocyte; ITGAM Ab, ITGAM neutralizing antibody.

Fig. 6

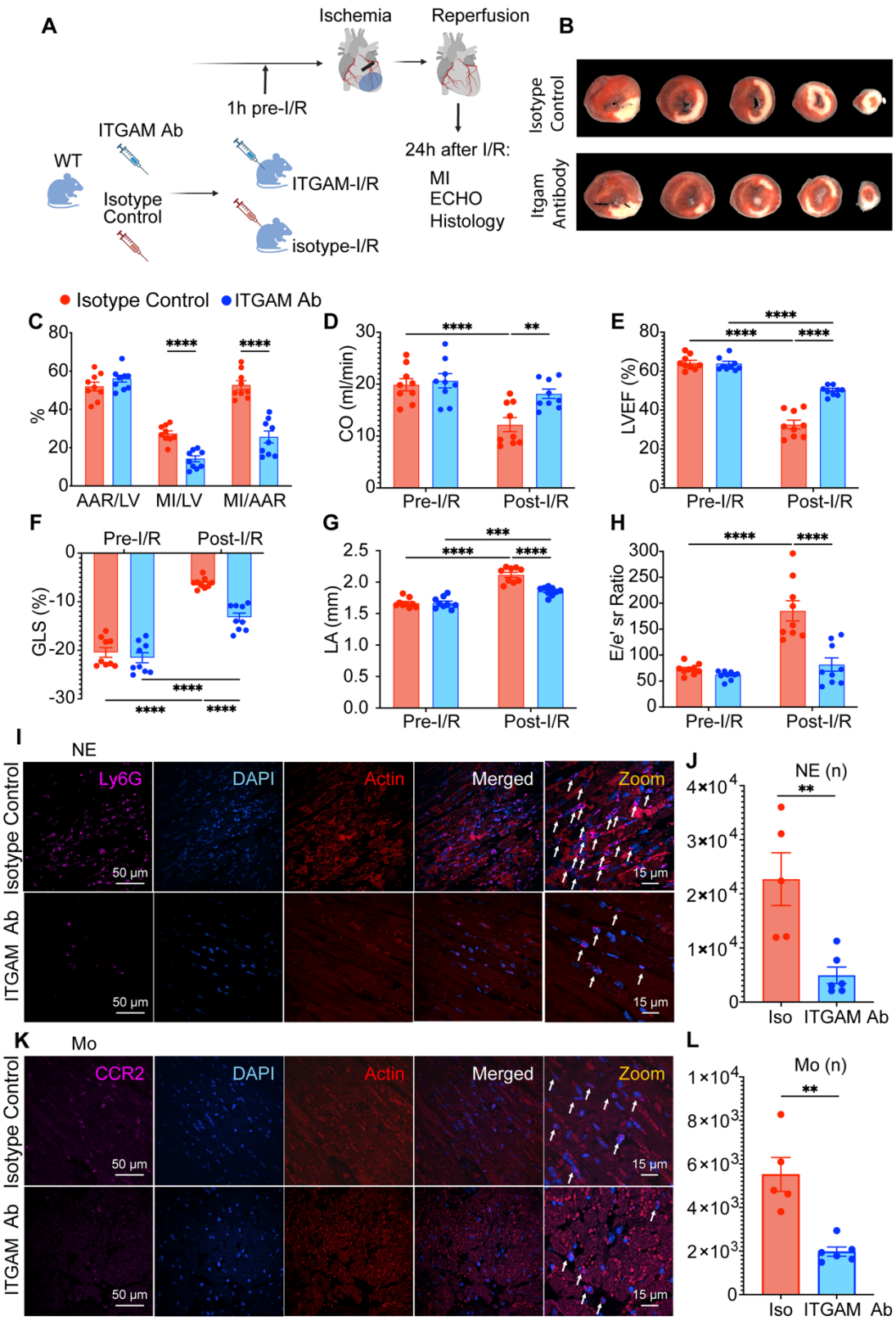
A
Ischemia
Reperfusion
1h pre-I/R
ITGAM Ab
WT
Isotype Control
ITGAM-I/R
isotype-I/R
24h after I/R:
MI
ECHO
Histology
B
Isotype Control
Itgam Antibody
Isotype Control
ITGAM Ab
C
%
AAR/LV
MI/LV
MI/AAR
D
CO (ml/min)
Pre-I/R
Post-I/R
E
LVEF (%)
F
GLS (%)
G
LA (mm)
H
E/e' sr Ratio
I
NE
Ly6G
DAPI
Actin
Merged
Zoom
50 μm
15 μm
J
NE (n)
Iso
ITGAM Ab
K
Mo
CCR2
L
Mo (n)

Figure 6. ITGAM neutralization attenuates leukocyte infiltration and limits ischemic MI. A, Study diagram for intraperitoneal administration of ITGAM neutralizing antibody or control isotype in a mouse model of MI and various experimental endpoints (n = 9 mice per group). **B**, Representative images of MI areas after triphenyl tetrazolium chloride (TTC) staining. **C**, Quantification of AAR/LV, MI/LV, and MI/AAR 24 hours after I/R. **D-E**, Cardiac output (CO) (**D**) and left ventricular ejection fraction (LVEF) (**E**). **F**, Echocardiography speckle tracking imaging showing global longitudinal strain (GLS). **G-H**, Echocardiographic data depict LA diameter (**G**), and E wave to reversed longitudinal strain rate ratio (E/e' sr) (**H**). **I and K**, Immunofluorescence staining of heart sections to show sarcomeric actin (red), and Ly6G/CCR2 (magenta). DAPI was stained in blue. **J & L**, Quantification of the cardiac infiltrated NE and Mo after I/R injury. Data shown are means ± SEM. Two-way ANOVA was used to test statistical significance. **P < 0.01, ***P < 0.001, ****P < 0.0001. I/R, ischemia-reperfusion; Enpa, enpatoran; ECHO, echocardiography; CO, cardiac output; LVEF, left ventricular ejection fraction; GRS, global radial strain; LA, left atrium; E/e' sr, mitral valve E wave velocity and reversed longitudinal strain rate ratio; NE, neutrophil; Mo, monocyte.

Fig. 7

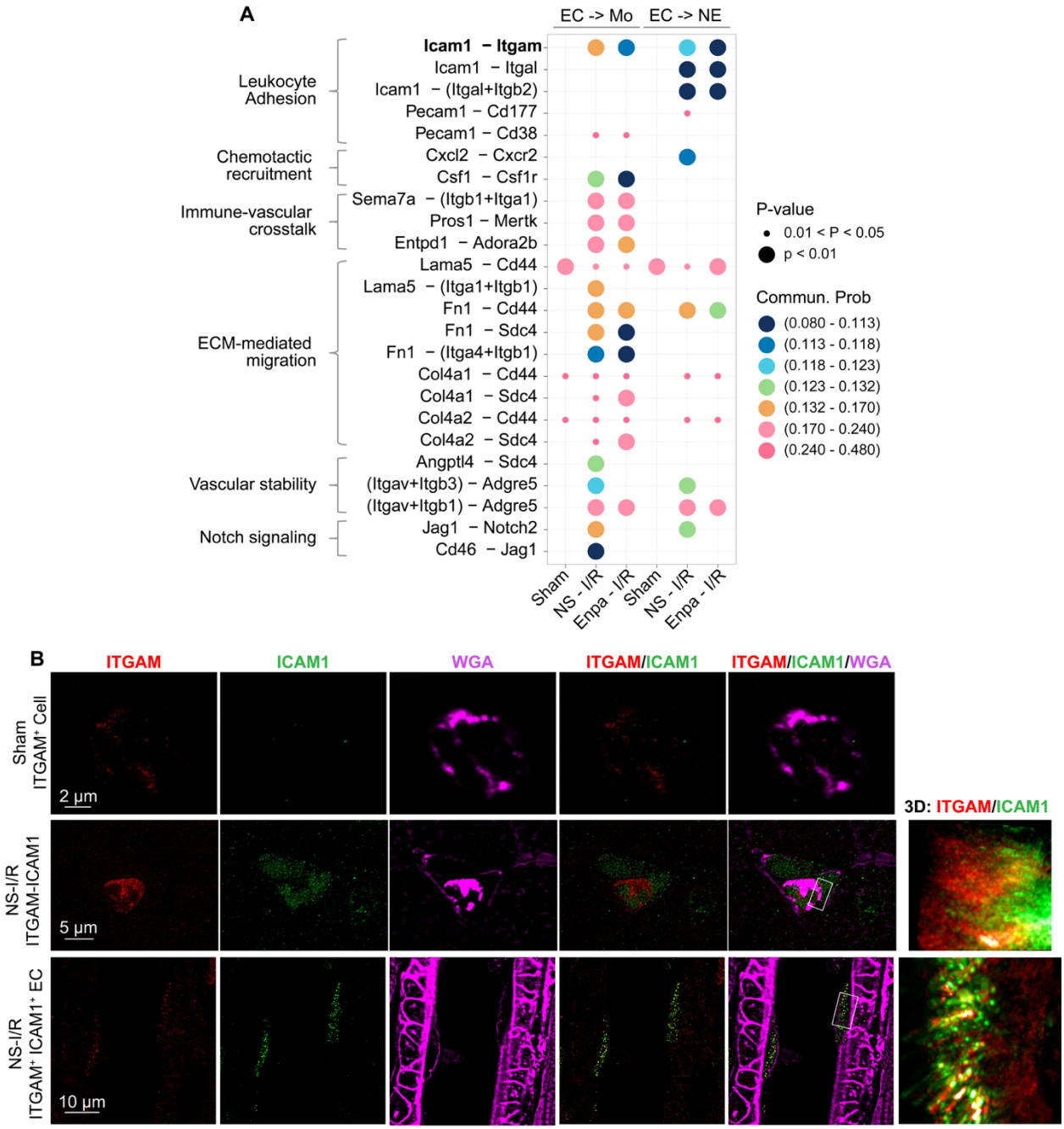

Figure 7. Myocardial I/R enhances ICAM1–ITGAM interaction. A. *In silico* ligand–receptor (L–R) interaction analysis of the snRNA-seq dataset. The 24 listed L–R pairs are associated with inflammatory and immune-related functions. Communication probabilities via L-R pair interaction between endothelial cells (ECs) and neutrophils (NEs) or monocytes (Mos) across sham, NS-I/R, and Enpa-I/R groups are shown. Each dot represents an individual L–R pair, with color indicating communication probability and dot size reflecting statistical significance (*P* value). Key endothelial-to-immune interactions, **Icam1–Itgam**, are bolded, revealing the dynamic changes in communication in response to I/R and to enpatoran treatment. **B,** STED super-resolution immunofluorescent images of heart sections to show ITGAM (red), ICAM1 (green), and cell

membranes (WGA, magenta). ICAM1–ITGAM colocalization was observed within endothelial junctional membrane protrusions in I/R mice. I/R, ischemia-reperfusion; Mac-1, Itgam + Itgb2; NS, normal saline; Enpa, enpatoran; EC, Endothelial cell; Mo, monocyte; NE, neutrophil; WGA, Wheat Germ Agglutinin.

Fig. 8

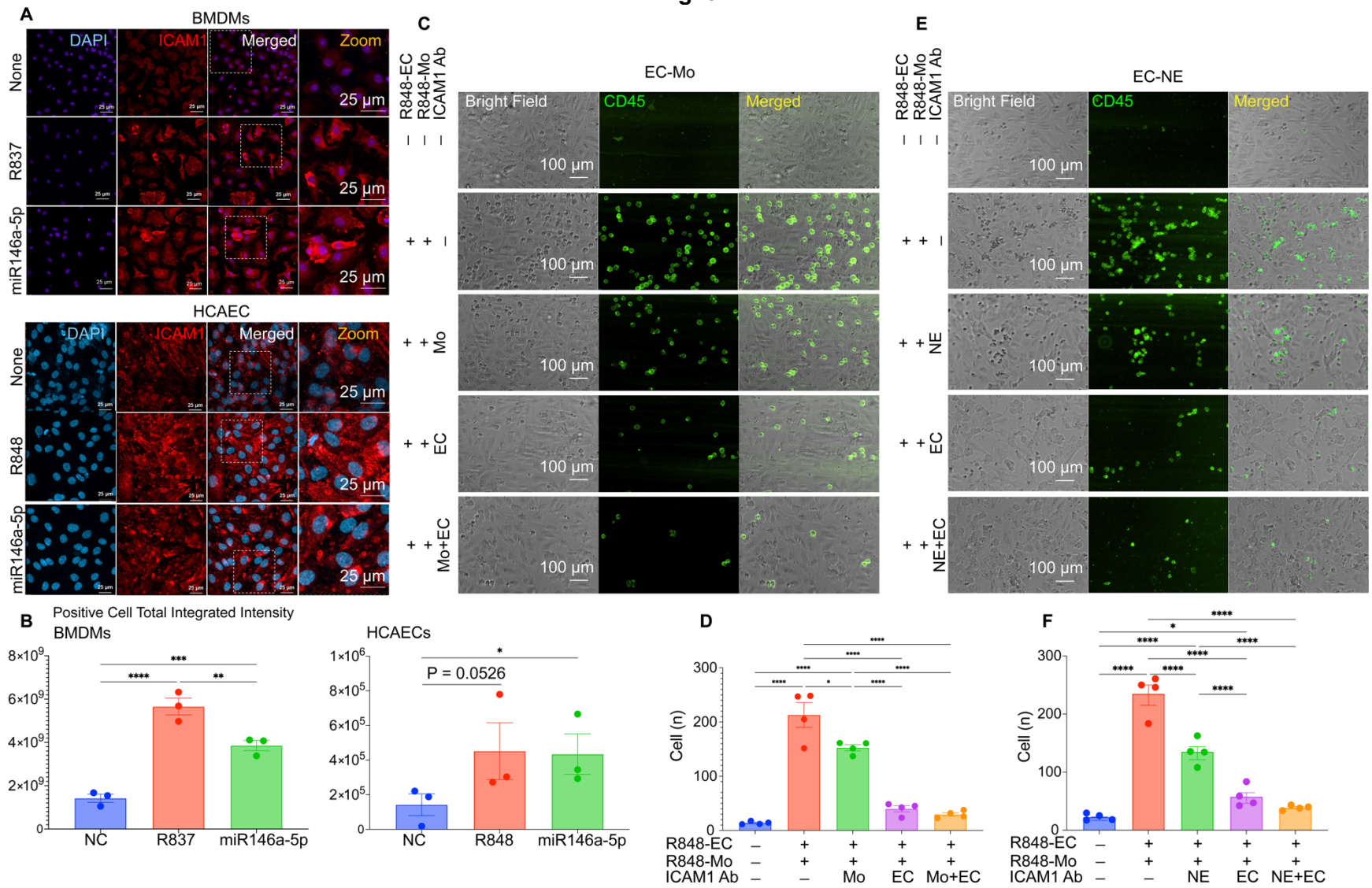
A
BMDMs
DAPI
ICAM1
Merged
Zoom
None
R837
miR146a-5p
25 μm
HCAEC
R848
C
EC-Mo
R848-EC
R848-Mo
ICAM1 Ab
Bright Field
CD45
Merged
100 μm
Mo
EC
Mo+EC
E
EC-NE
NE
NE+EC
B
Positive Cell Total Integrated Intensity
BMDMs
HCAECs
P = 0.0526
NC
R837
miR146a-5p
R848
D
Cell (n)
Mo
EC
Mo+EC
F
NE
EC
NE+EC

Figure 8. TLR7 activation promotes ICAM1 expression and leukocyte–endothelial interaction. A, The representative images of ICAM1 expression in BMDMs and HCAECs. **B,** Quantification of the ICAM1^{+} cell total integrated intensity. **C-D,** Microfluidic adhesion assay of THP-1 (Mo) adhesion to HCAEC (**C**) and quantification (**D**) under different treatment conditions. **E-F,** Microfluidic adhesion assay of human fresh neutrophil adhesion to HCAEC (**E**) and quantification (**F**) under different treatment conditions. Treatment time for R848/enpatoran: 3h for Mo, 18h for EC; ICAM-1 Ab: 1h. Adherent CD45^{+} cells appear as discrete green puncta, while continuous green streaks reflect perfused monocytes under flow conditions. Data shown are means ± SEM. A one-way ANOVA was used to test for statistical significance. *$P < 0.05$, **$P < 0.01$, ***$P < 0.001$, ****$P < 0.0001$. NC, nontreatment control; DAPI, 4′,6-diamidino-2-phenylindole; BMDMs, bone-marrow-derived macrophages; HCAEC, human coronary artery endothelial cell; Integrated intensity, the sum of pixel intensities within a designated area of a cell; ICAM1 Ab, ICAM1 neutralizing antibody; Mo, monocyte; NE, neutrophils.